Pergamon

Int. J. Heat Mass Transfer. Vol. 39, No. 5, pp. 965–973, 1996
Elsevier Science Ltd
Printed in Great Britain

0017–9310(95)00173–5

Performance of direct-contact heat and mass exchangers with steam–gas mixtures at subatmospheric pressures

M. C. DE ANDRÉS,† E. HOO‡ and F. ZANGRANDO
National Renewable Energy Laboratory (NREL), 1617 Cole Boulevard, Golden, CO 80401, U.S.A.

(*Received* 7 *October* 1994 *and in final form* 16 *May* 1995)

Abstract—Tests were conducted to determine the performance of direct-contact heat and mass exchangers containing structured packings in field applications. The exchangers tested serve as intercoolers–condensers between the various stages of a vacuum compression train that discharges the exhaust gases from a low-temperature power plant. The gases, which consist of low-pressure steam and a mixture of noncondensible gases, are contacted with seawater as the coolant. The structured packing is more commonly used as fill in evaporative cooling towers, which operate at atmospheric pressure. These tests were conducted at absolute pressures between 1.6 and 16 kPa, and noncondensible mass fractions between 0.1 and 0.9, significantly extending the existing data base on condensers. The new data show the effect of high noncondensible mass fractions and superheat on the heat and mass transfer process. The results indicate that these exchangers can be designed to condense the steam to within a few percent of the theoretical limits, while attaining small temperature approaches, and incurring low pressure drops. Useful approximations to estimate their performance are discussed. The data were also used to validate detailed computer models, which accurately predict the heat and mass transfer over the entire range tested. These models can now be used with confidence for engineering design of condensers in geothermal and conventional power plants.

INTRODUCTION

The work described in this paper is a continuation of an intensive program initiated in 1981 at the Solar Energy Research Institute (SERI), now the National Renewable Energy Laboratory (NREL), to develop a data base on the performance of direct-contact heat exchangers (DCXs) and condensers (DCCs). The initial investigation focused on the low-pressure regime characteristic of heat exchangers proposed for open-cycle ocean thermal energy conversion (OC-OTEC) systems.

A significant body of information exists on DCXs. The majority of the work concentrates on spray, baffle-tray, sieve, and randomly packed columns for chemical processing and heat recovery, and is well summarized in [1, 2]. The thermal effectiveness of these DCXs, although higher than for surface exchangers, is still insufficient for low-temperature (e.g. OC-OTEC) applications. Therefore, contactors with even higher performance and lower gas pressure drops had to be found, and reliable design and prediction methods had to be developed and validated.

The tests reported here were conducted over a much broader set of conditions than previously tested, and provide new information into the pressure range of geothermal and conventional power plants. These data were used to (a) determine the thermal and condensing effectiveness of DCXs with structured packings, as a function of gas and cooling fluid inlet parameters and (b) to validate the computer models over the broader range of conditions.

The models [3] are one-dimensional, steady-state analytical models to calculate the heat, mass, and momentum transfer processes occurring in an exchanger that contains structured packing, in both cocurrent and countercurrent flows. The Chilton–Colburn heat- and mass-transfer analogy is used. The transfer correlations are adapted from a number of correlations existing in the literature, which were modified based on our early experimental data, as detailed in [3]. In the models, the process differential equations are integrated along the length of the exchanger to obtain local conditions of steam, noncondensible (NC) gases, liquid and dissolved gases. In the countercurrent geometry, the liquid enters from the top and the gas from the bottom. The countercurrent model integrates through the process equations by marching from the bottom to the top, based on an initial guess of the outlet liquid state. Iterations are carried out until the calculated water conditions at the top of the exchanger match the specified liquid inlet conditions, within a defined tolerance. Input to the models consists of typical design parameters such as: geometry of the packing and DCX; cooling fluid inlet temperature and mass flow (or liquid loading); gas composition (or total pressure), gas mass flow (or

† Sabbatical Professor from Grupo de Energía Solar, Facultad de Físicas, Universidad Complutense, 28040 Madrid, Spain.

‡ Author to whom correspondence should be addressed.

NOMENCLATURE

C_p	specific heat [J kg^{-1} K^{-1}]
F	actual fraction of steam mass condensed, equation (10)
F_{id}	ideal fraction of steam mass condensed, equation (3)
H	ratio of sensible to latent heat, equation (7)
h_{fg}	latent heat of condensation [J kg^{-1}]
Ja	Jakob number for heat and mass exchange, equation (6)
Ja_0	Jakob number for condensation, equation (5)
L	liquid loading (mass flow per overall cross-sectional area of intercooler) [kg m^{-2} s^{-1}]
m	mass [kg]
P	total absolute pressure [Pa]
pp	partial pressure of gas component [Pa]
S	steam loading (mass flow per overall cross-sectional area of intercooler) [kg m^{-2} s^{-1}]
T	temperature [°C, K]
T_{dew}	dew-point temperature [°C, K]
T_{sat}	adiabatic saturation temperature [°C, K]
T_{super}	superheat [°C, K]
T_{wb}	wet-bulb temperature [°C, K]
X	mass fraction of species to total mass of gas
Y	mole fraction of species to total mass of gas.

Greek symbols

ε_c	thermal effectiveness for condensation, equation (9)
ε_n	thermal effectiveness for heat exchange, equation (9)
Δ	difference in quantity (D in figures).

Subscripts

1–5	intercooler number
c	condensed, condensation
g	gas
h	heating/cooling
i	in, inerts (noncondensibles)
o	out
s	steam
th	theoretical
w	water, seawater.

Superscript

*	equilibrium value.

gas loading), dew-point temperature, and superheat. The gas can actually be characterized in various equivalent ways, either directly or calculated from measured quantities via the gas law, as described later.

The models were first validated with experimental data using fresh water at SERI/NREL [3] and then using seawater at the U.S. Department of Energy's Seacoast Test Facility, on the big island of Hawaii [4]. Both cocurrent and countercurrent geometries were tested, and the most relevant results are summarized in ref. [5]. These tests were carried out at pressures between 0.9 and 2.5 kPa, NC gas fractions of less than 0.02 in cocurrent and less than 0.3 in countercurrent exchangers, and negligible superheat of the inlet gases. The tests reported here also were conducted at the Hawaii facility and extended the data base on countercurrent units to pressures up to 16 kPa, inlet NC fractions up to 0.9 and inlet gas superheat up to 90°C.

OVERALL SYSTEM LAYOUT AND LIMITATIONS

An operating OC-OTEC power plant [6] was selected as a convenient source of the gas mixture for these tests. The flow of the gas stream through this plant is sketched in Fig. 1(a). The tests were carried out in the four intercoolers (IC) between each stage of compression (C). A representative IC layout is shown in Fig. 1(b).

In the OC-OTEC system, steam is produced at around 2.4 kPa from warm seawater, typically at about 25°C, and is condensed on deep-ocean cold seawater, typically at 5°C. At these pressures, most of the NC gases dissolved in the warm and cold seawater come out of solution. These gases are primarily nitrogen and oxygen, in total dissolved concentrations around 19 ppm. Ambient air leakage into the system is an additional source of noncondensibles. Because this power plant operates at subatmospheric pressures, the NC gases must be pumped out to maintain operating pressures. To be efficient, the process usually requires several stages of compression with intercooling–condensing between these stages.

The main components of the OC-OTEC power-producing system in Hawaii [6] are contained in a concrete vessel that incorporates the concentric evaporator and condenser, and the radial inflow turbine. Design warm- and cold-seawater mass flows are 620 kg s^{-1} and 420 kg s^{-1}, respectively. At design conditions, steam is flashed and condensed at a rate of 3.5 kg s^{-1}. The steam flows through the turbine–generator assembly to produce electric power and then to the main condenser, which is composed of one cocurrent and one countercurrent stage. About 99% of the steam is condensed here; the remainder cannot be condensed at the low pressures in the main condenser because NC gases are present. The gas at the exhaust of the countercurrent stage is routed to the vacuum compression train which consists of five

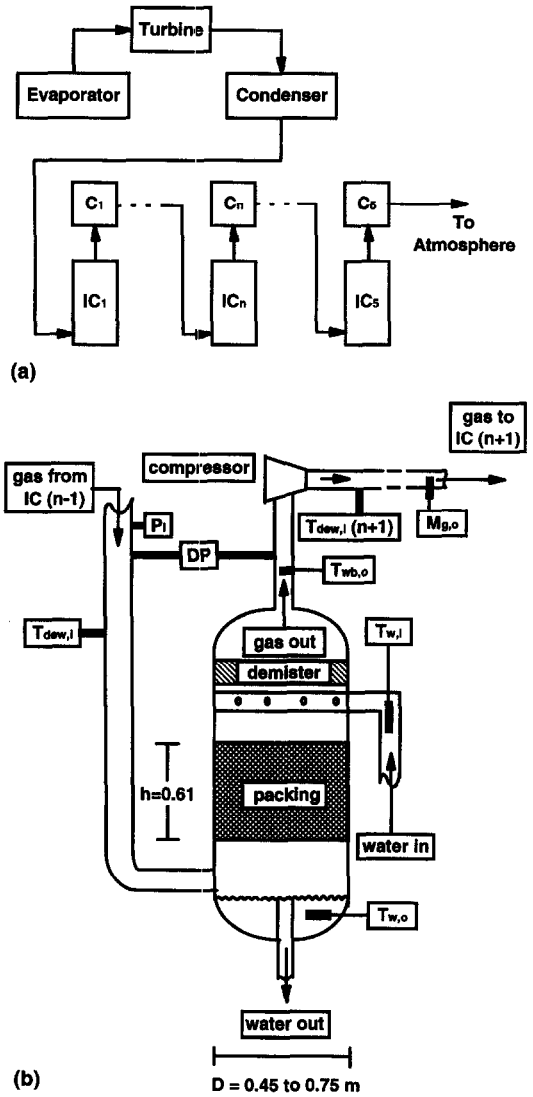

Fig. 1. (a) Schematic of OTEC system gas flow. (b) Typical layout and location of instrumentation for intercooler IC*n* (one of four, in series). Not to scale.

stages in series. The first four stages are custom-made centrifugal compressors; the first stage consists of three identical units in parallel. The design compression ratio of each stage is about 2. Each stage is outfitted with a variable-frequency drive, allowing them to operate over a range of compression ratios and mass flow rates. The fifth stage is a commercial, constant-volumetric-flow compressor that works over a wide range of inlet pressures. Between each stage of compression, a direct-contact intercooler is used to condense a portion of the remaining steam and to cool the gas to reduce the work load of the following compressor. Typically, the gas at the outlet of each unit is brought to near-equilibrium conditions with the incoming water, at the operating pressure of that intercooler. The total mass flow of gases at the exit of the compressor system is 21 g s^{-1} at design conditions, with a steam content on the order of 1 g s^{-1}.

Because a single gas stream flows through the compression train and the ICs, the system is highly coupled. Changes in one component have a significant effect on conditions downstream, therefore serious limitations were imposed on the possible test matrix. For example, it was impossible to obtain simultaneously high steam flows, high total pressures, and low NC flows (three conditions characteristic of power-plant condensers). To achieve a wide range of conditions in these tests, the entire system was forced to operate under unusual conditions. For example, it was sometimes necessary to reduce drastically the flow of cold water in one IC to force evaporation and provide additional steam to the following IC.

EXPERIMENTAL EQUIPMENT

Figure 1(b) is a schematic of the flow geometry in the four intercoolers, showing the primary measurements made, and the placement of the sensors used in the experiments. The tests were carried out on the intercoolers numbered IC2–IC5. The diameter of IC2–IC5 varied as shown (30, 20, 18, 18 inches, respectively).

The gas mixture coming from the previous compressor enters near the bottom of the IC and the cold seawater enters near the top, in a countercurrent-flow arrangement. A height of only 0.61 m (2 ft) of metal structured packing (Koch AX) was used in the intercoolers. This packing was selected primarily because of the high gas temperatures expected. The surface-area-to-volume ratio for this packing is 250 $m^2\ m^{-3}$. A chevron mist eliminator is installed above the circular water distributor to reduce seawater droplet carryover into the compressors. The ICs are insulated to just beyond the inlet water temperature sensor and down to the point of seawater discharge. Leak checks were performed on the overall system to verify negligible ambient air leakage. Table 1 shows the range of conditions obtained in each IC; note the overlapping data ranges for several ICs, providing duplicate data points from different ICs for the analysis.

PRIMARY MEASUREMENTS, UNCERTAINTY ESTIMATES AND INSTRUMENTATION

The type and location of the instrumentation were selected based on spatial and operational constraints of the existing equipment. Some redundancy was built into the selection of instrumentation, to ensure that sufficient data would be available for analysis. All possible combinations of measurements were assessed during the initial phase of data analysis, and consistent primary measurements for all ICs were selected to provide the smallest overall errors, principally for the fraction condensed. These primary measurements, or values calculated from them using the gas law, are used for calculation of all performance parameters and model input.

For each IC, the selected primary measurements

Table 1. Range of measurements and parameters attained in each intercooler and uncertainty estimate for primary measurements

Range	IC no.	P_i [Pa]	S_i [kg m^{-2} s^{-1}]	$X_{i,i}$	$T_{dew,i}$ [°C]	$T_{w,i}$ [°C]	ΔT_c [°C]	T_{super} [°C]	DP [Pa]	F
min	2	1635	0.01	0.10	11.3	5.62	5.3	0	6	0.65
max	2	4881	0.26	0.70	18.8	6.58	12.5	68	132	0.94
min	3	3027	0.01	0.60	12.8	5.81	1.1	29	−20	0.13
max	3	5602	0.06	0.81	21.6	20.43	8.9	83	44	0.58
min	4	4917	0.01	0.52	15.9	5.88	1.9	19	−6	0.20
max	4	9755	0.07	0.88	24.6	20.77	12.2	89	38	0.62
min	5	6965	0.00	0.70	6.5	6.26	0.3	0	14	0.00
max	5	15843	0.03	0.93	23.1	20.76	10.8	67	95	0.52
Worst-case uncertainty estimates (±)		60 Pa			0.5°C	0.05°C	0.5°C	5°C	15 Pa	

are P, ΔP, $T_{w,i}$ and $T_{dew,i}$; NC mass flow is calculated from $m_{g,o}$, measured at the exit of the compression train [see Fig. 1(b)]. Steam flow is calculated from the NC flow and steam fraction, which is obtained from T_{dew} and P. The dew point at the inlet of the following IC is used to determine the steam fraction of the gas out of the IC considered, assuming no mass exchange through the compressor. This measurement was selected because it provided the most consistent data, especially at the lower total pressures. Only for the last intercooler (IC5), $T_{wb,o}$ was used to determine the outlet steam mass flow, because no other dew-point sensor was available.

Estimated maximum uncertainties of the primary measurements are shown at the bottom of Table 1. All sensors were custom calibrated by the manufacturer just prior to the experiments. Post-test recalibration of the sensors was not done; therefore, the uncertainty estimates account for the maximum possible zero, span and temperature drift of the sensor since the time of calibration, as well as other potential sources of errors such as thermistor self-heating, fluctuations of sampling flow to the dew-point sensors, and curve-fitting inaccuracies. Overall uncertainties on calculated parameters are discussed with the results.

Data were collected continuously but stored only after the system had approached steady-state. Ten consecutive readings of each sensor were taken during one scan, as the data acquisition system scanned through all sensors in a one-minute period. Typically, five or more consecutive scans were averaged for each data 'point' reported here. The overall uncertainty estimates shown in Table 1 refer to these averaged data points.

Data were collected with a Keithley 2001 multimeter and 7001 multiplexer, operated by a laptop computer using National Instruments LabView software. The available instrumentation consisted of capacitance pressure sensors (Rosemount 3051CA and 1151AP for absolute pressures, 3051CD and 1151DR for differential pressures); chilled-mirror hygrometers for inlet dew-point temperatures (General Eastern E1A, 1111H-SR sensors); thermistors for all other temperatures (YSI SP20228, custom four-wire ultrastable probes, 5 kΩ at 25°C); a thermal dispersion sensor for total mass flow of gas out of the system (Fluid Components Intl. AF88); turbine meters for seawater volumetric flows (Flow Technology Inc. FT16 and FT32, with ceramic journal bearings and frequency pick-off).

The chilled-mirror hygrometers have uncertainties of ±0.2°C at steady sampling pressures. Flow through these sensors was provided without pumps by connecting the return of each sampling loop to the point of lowest pressure on the system. This resulted in flow oscillations in the sample lines for IC2 and IC3, which have low driving-pressure differences. Location of the sampling taps was also not optimal. In some cases, fluctuations of individual dew-point readings up to ±1°C were observed, resulting in the overall uncertainty estimates, on the averaged sets, as shown in Table 1. Better control of sampling flows is recommended for future tests.

The mass of noncondensible gases that flow through the ICs is calculated from the measured exhaust-gas mass flow rate ($m_{g,o,5} = m_{s,o,5} + m_i$). Release of dissolved NC gases in the ICs and ambient leakage are negligible; therefore, m_i is constant through the system. The uncertainty on $m_{g,o,5}$ is less than ±3% of flow. The fraction of steam is calculated from the total pressure and from the saturation pressure equivalent to the measured wet-bulb temperature, assuming saturated gas at the outlet of IC5. Because the gas actually exits slightly superheated, this assumption predicts a mass of steam at the exit of IC5 larger than the actual value. This results in a bias error in the calculated value for $m_{s,o,5}$, so m_i is always underestimated in all the ICs. Taking this bias conservatively as a random error, the measurement and the assumptions give a maximum overall uncertainty on m_i of ±1.0 g s^{-1} (about ±5% of typical NC flows).

No attempt was made to measure gas temperatures because of the very large errors expected at such low pressures. Inlet gas temperatures were calculated from

measured compression ratios, design compressor efficiencies, and assuming saturated conditions at each IC outlet. The model predictions indicate that the gas should actually exit superheated by a few degrees. Therefore, the total uncertainty in the calculated gas temperatures is expected to be about $\pm 5°C$.

Ambient temperature was measured with a thermistor. These sensors were also used for a 'wet bulb' measurement at the outlet of each IC; however, this measurement proved unreliable. A similar assembly (a wetted-wick RTD probe) had provided wet-bulb temperatures to better than 0.1°C in previous tests [3], but they were carried out with a saturated gas at lower pressures and lower NCs. The reduced mass transfer at the conditions reported here is apparently insufficient to maintain the probe near the adiabatic saturation temperature, even though the Lewis number is near one. Further analysis is required to resolve the noted discrepancies.

Worst-case uncertainties on water flow rates are $\pm 3\%$ at the lowest flow ranges of each sensor. A heat balance on the (narrow) intercoolers was not used to determine steam flow because the variable ambient heating during the day, and the large uncertainty on gas temperature resulted in larger errors on the calculated mass flows than using other methods.

PERFORMANCE PARAMETERS

The performance of direct-contact, countercurrent exchangers is a complex function of liquid and gas loading, temperature driving potential, inlet noncondensible-gas concentration, inlet dissolved gas concentration, inlet dew-point temperature, superheating, and geometry. The fraction condensed, based on Jakob number and thermal effectiveness, is the main parameter selected to describe the thermal performance of the ICs, and these are defined below. Overall pressure drop through the packing and temperature approach at the gas outlet (equivalent to venting ratio [4, 5]) are also discussed with the results.

Temperature driving potentials for condensation and for sensible heat exchange

For a superheated mixture of steam and noncondensible gases, the dew-point temperature is lower than the adiabatic saturation temperature T_{sat}. If this mixture is contacted with liquid water, the maximum temperature that the water can attain corresponds to the temperature of thermodynamic equilibrium with the gas phase, T_{sat}. The simultaneous heat and mass exchange process can be described in terms of total enthalpy transferred or it can be separated into mass and sensible heat components. The second is more useful to describe these exchangers.

The overall theoretical driving potential is $\Delta T_{th} = (T^*_{sat,i} - T_{w,i})$.† However, once the cooling water reaches temperatures above $T^*_{dew,i}$, the additional sensible heat that can be removed from the gas phase is used principally for mass transfer from the liquid water back into the gas phase; so this additional steam must be recondensed further along in the exchanger.

For *net* mass transfer, the effective condensation driving potential, driven by partial-pressure differences, can be expressed as

$$\Delta T_c = T^*_{dew,i} - T_{w,i}. \tag{1}$$

For sensible heat transfer, the temperature driving potential is

$$\Delta T_h = T_{g,i} - T_{w,i}. \tag{2}$$

Fraction condensed

The fraction condensed is defined as the ratio between the mass of steam condensed and the total mass of steam entering each intercooler: $F = (m_{s,i} - m_{s,o})/m_{s,i}$. Under ideal conditions (when there is no gas pressure drop, the gas mixture behaves as a perfect gas, the mass of noncondensibles remains constant and the steam exits in equilibrium with the entering seawater) the fraction condensed reaches its maximum possible value

$$F_{id} = \left[1 + Y_{i,i}\frac{pp_{s,o}(T_{w,i})}{pp_{s,i}(T^*_{dew,i}) - pp_{s,o}(T_{w,i})}\right]^{-1}. \tag{3}$$

If the inlet molar concentration of noncondensibles $Y_{i,i}$ is zero, then $F_{id} = 1$. If $Y_{i,i}$ is high, as in these tests, F_{id} can be significantly lower than one, because some steam must be exhausted from the exchanger with the NC gases. It is important to note that the steam and liquid loadings do not enter into equation (3) because it is assumed that the amount of water available in the IC is greater than the ideal limit (i.e. $Ja \geqslant 1$, see below). Note that F_{id} is greatly influenced by $X_{i,i}$ and by the difference in the two temperatures, ΔT_o, but not significantly by the temperatures themselves.

Jakob number

The Jakob number describes the minimum amount of water needed to condense the steam and to cool the gas to the ideal limits [3, 4]. Using the driving potentials defined in equations (1) and (2), the heat-balance equation under ideal conditions gives

$$\dot{m}_w C_{p,w}(T^*_{dew,i} - T_{w,i}) = F_{id}\dot{m}_{s,i}h_{fg} + \dot{m}_{g,i}C_{p,g}(T_{g,i} - T_{w,i}) \tag{4}$$

assuming that the latent heat and the heat capacities of the liquid and of the overall gas mixture remain constant. For the limiting case of a saturated gas ($T_{dew} = T_{sat}$) and in the absence of NC gases, all the steam can theoretically be condensed. Rearranging the heat-balance terms in equation (4) gives the (condensation) Jakob number

$$Ja_0 = \frac{LC_{p,w}(T^*_{sat,i} - T_{w,i})}{Sh_{fg}} \tag{5}$$

† The superscript (*) implies use of the proper saturation curve. For steam and seawater, this "boiling point" correction is about +0.28°C above fresh water temperature in the pressure range examined.

where L and S are the inlet liquid and steam loadings (water and steam mass flows per unit cross-sectional area of the IC, respectively). The theoretical limit of Ja_0 is one and the minimum liquid loading required is calculated from equation (5) by equating the two heat-balance terms (in the ideal case, the entire driving potential is available to condense all the steam). Real exchangers need more flow for the same conditions, so they operate at $Ja_0 > 1$.

For a superheated gas with noncondensibles present, the Jakob number is

$$Ja = \frac{LC_{p,w}\Delta T_c}{Sh_{fg}(F_{id}+H)} = \frac{Ja_0}{(F_{id}+H)} \tag{6}$$

where H is the ratio of the maximum sensible heat that can be removed from the gas with respect to the required latent heat to condense *all the entering steam*, and is expressed as

$$H = \left[C_{p,s} + C_{p,i}\frac{X_{i,i}}{(1-X_{i,i})}\right]\frac{\Delta T_h}{h_{fg}}. \tag{7}$$

Thermal effectiveness

The thermal effectiveness is a parameter that indicates the approach to ideal conditions. Because latent and sensible heating must be removed from the gas phase, two thermal effectivenesses are defined.

In parallel to equation (4), the heat balance for actual conditions becomes

$$\dot{m}_w C_{p,w}(T_{w,o}-T_{w,i}) = F\dot{m}_{s,i}h_{fg} + \dot{m}_g C_{p,g}(T_{g,i}-T_{g,o}). \tag{8}$$

The thermal effectivenesses are

$$\varepsilon_c = \frac{T_{w,o}-T_{w,i}}{\Delta T_c} \quad \varepsilon_h = \frac{T_{g,i}-T_{g,o}}{\Delta T_h}. \tag{9}$$

The first defines the *thermal effectiveness for condensation*. It compares the observed temperature difference in the cooling water with the available temperature driving potential, if sensible heat transfer is negligible. The second defines the *thermal effectiveness of a heat exchanger*, relating the temperature difference observed in the gas phase with the available temperature driving potential for sensible cooling.

Dividing equation (8) by the latent heat required to condense all the steam coming into the IC and incorporating the effectivenesses, the actual fraction condensed for a heat and mass exchanger is

$$F = \varepsilon Ja = \varepsilon_c Ja_0 - \varepsilon_h H. \tag{10}$$

The limit for the simple condenser is $F = \varepsilon_c Ja_0$. In power-plant applications, $X_{i,i}$ is typically much less than 0.1 so countercurrent DCCs with structured packing give essentially a constant F (about 0.95) and a thermal effectiveness inversely proportional to the Jakob number selected [5].

DATA COLLECTED

Data were taken on all four intercoolers for each operating condition established in the system, resulting in four data sets per test. However, not all these data sets can be used for analysis. To approach the desired conditions, evaporation was induced in some units to provide additional mass flow to downstream ICs. As a result, data sets in which evaporation was occurring were useless for model validation and were eliminated. This accounted for the majority of the eliminated data sets. A few others were discarded because the dew-point temperature was near or above ambient temperature, implying potential condensation in the sampling lines. Some were eliminated because of large errors in the calculation of the mass condensed. This was particularly true for IC5, where the range of incoming mass of steam was between 0.6 and 5 g s^{-1} and the fraction of NC gas ranged from 0.7 to 0.9. This large ratio of NC gases meant that only a very small fraction of the incoming steam could be condensed, leading to large errors. Two sets were eliminated because the computer model did not converge at those conditions. In some units, compressor and sensor failures also negated data collection at times.

This resulted in a data base of 104 points for validation of the direct-contact countercurrent model.

ANALYSIS OF RESULTS

Figure 2(a) shows the experimental fraction of steam condensed versus that predicted by the model, for IC 2, 3 and 4. The experimental result is calculated from inlet and outlet measurements, and in this case F_{exp} is calculated using $T_{dew,i}$ and $T_{dew,o}$. The model uses the following inlet parameters: $T_{dew,i}$, $T_{w,i}$, L, S, $X_{i,i}$ which are either measured directly or calculated as described previously. A point below the parity line implies that the model overpredicts the actual fraction condensed. Because the inlet parameters are the same for both, all the errors associated with the primary measurements are assigned only to the experimental values. The estimated overall uncertainty on F depends on the operating conditions, but it is less than $\pm 6\%$ of the calculated F for all except four points on the graph. These four points fall outside the band of predictions, but no reason was found to explain the discrepancy. The uncertainty band for each of these points is shown separately in the figure. Overall, good agreement exists between experiments and model prediction, and the experimental results for F deviate from the parity line by a standard deviation of ± 0.046 for all the data shown. $X_{i,i}$ reaches nearly 0.9 and P reaches nearly 10 kPa in the data shown here (see Table 1 for ranges covered in each IC). The model predicts equally well at high and low $X_{i,i}$.

Figure 2(b) shows the same for IC5, but here the experimental fraction condensed is calculated using the inlet dew-point temperature and the outlet wet-

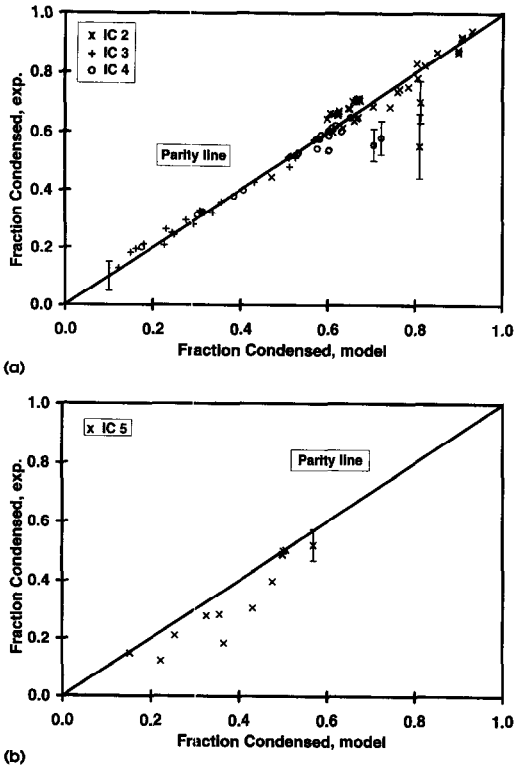

Fig. 2. Experimental fraction condensed vs fraction condensed predicted by the computer model for (a) IC 2, 3 and 4 (standard deviation of data from the parity line is ± 0.046), and (b) IC 5 (standard deviation of data from the parity line is -0.075).

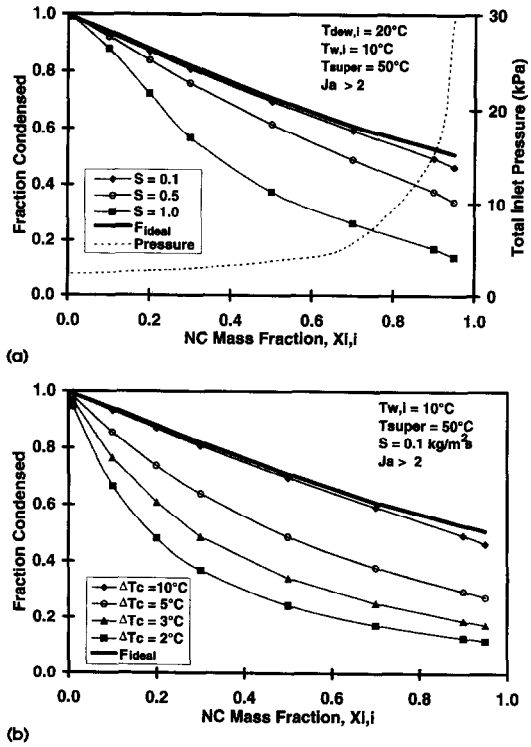

Fig. 3. Parametric dependence of actual and ideal fraction condensed for fixed inlet conditions but (a) varied steam loading S (kg m^{-2} s^{-1}) and (b) for $S = 0.1$ kg m^{-2} s^{-1} but varied driving potential.

bulb temperature (no outlet dew point was available). Saturated outlet conditions are assumed because outlet gas temperature was not measured. This overestimates the mass of steam that exits this IC, resulting in a lower than actual fraction condensed. The standard deviation of the data from the parity line is -0.075. This higher value for IC5 is partially due to the small masses of steam in IC5, and to the error associated with the wet-bulb measurement.

The experimental fraction condensed for all the intercoolers is within a standard deviation of ± 0.055 from the ideal limit F_{id}, even up to $X_{i,i} = 0.9$. This is expected because direct-contact exchangers are very effective and because these ICs were designed to operate at low steam loadings.

Because of the good agreement between model predictions and experimental results, a parametric analysis was conducted with the model for fixed inlet conditions, to clarify the salient features of these exchangers. The strongest dependence of the fraction condensed is on NC fraction, steam loading, available temperature driving potential, and Jakob number.

Figures 3(a) and (b) show ideal and predicted fraction condensed for a countercurrent exchanger, as a function of inlet NC fraction. Figure 3(a) is for the particular case of $T_{dew,i} = 20°C$ and variable S. Total pressure is defined by T_{dew} and $X_{i,i}$ but is not a function of S, so it is represented by the dashed line with scale to the right. The ideal fraction condensed [equation (3)] is also not a function of S, and it drops off almost linearly until $X_{i,i} > 0.95$. Instead, the actual fraction condensed is very sensitive to both $X_{i,i}$ and S. For $X_{i,i} > 0.95$ all the curves drop rapidly to zero as the pressure goes to infinity. The model cannot predict correctly the behavior as P goes to infinity but good agreement with data was demonstrated [see Figs. 2(a) and (b)] for $X_{i,i}$ up to 0.9.

Figure 3(a) shows the progressive deviation of the actual fraction condensed from the ideal condensation limit as S increases, when ΔT_c is fixed. For low S over the entire range of noncondensible concentrations, F remains close to F_{id}, so equation (3) can be used to estimate the condensation performance. For very low $X_{i,i}$, F is approximately equal to F_{id}, for one order of magnitude change in S.

For a given steam loading, gas pressure drop increases nearly quadratically with $X_{i,i}$ because of the additional gas that must flow through the same cross-sectional area of the exchanger. For low $X_{i,i}$, when the total gas pressure drop is small, F is strongly influenced by an increase in $X_{i,i}$. For high $X_{i,i}$, the gas pressure drop is much higher and the effect of additional NC gas is less noticeable, reducing the slope of the F curve.

The system is equally sensitive to ΔT_c as it is to S, as shown in Fig. 3(b). The curve for $\Delta T_c = 10°C$ is

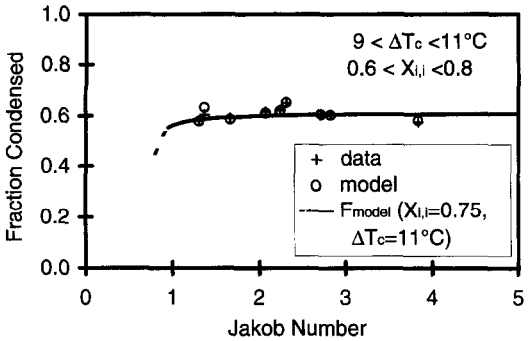

Fig. 4. Dependence of fraction condensed on Jakob number. Model predictions are for constant inlet conditions: $X_{i,i} = 0.75$, $S = 0.05$ kg m^{-2} s^{-1}, $\Delta T_c = 11°C$, $T_{w,i} = 10°C$, $T_{super} = 80°C$. Data points near these conditions and their corresponding model prediction are also shown.

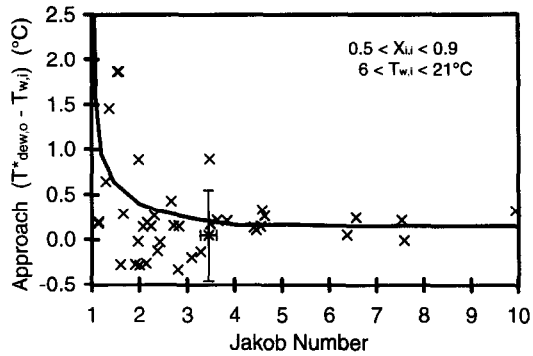

Fig. 5. Approach between steam and seawater at the gas outlet of the intercooler. The solid line is the outer envelope of model predictions.

the same as the curve for $S = 0.1$ kg m^{-2} s^{-1} in the previous figure. For very small $X_{i,i}$, the exchanger operates well, condensing nearly all the entering steam even at $\Delta T_c = 2°C$. For higher $X_{i,i}$, much higher driving potentials are necessary to condense the maximum possible quantity of entering steam.

The effect of Jakob number on fraction condensed is shown in Fig. 4. The model is used once again to show this dependence more clearly. For a fixed inlet condition with $X_{i,i} = 0.75$ and $\Delta T_c = 11°C$, model predictions for F as a function of Ja are given by the curve. As Ja increases beyond a value of unity, the actual fraction condensed rapidly approaches F_{id} for that fixed inlet condition. A further increase in Ja results in a smaller and smaller incremental fraction of the steam being condensed at the expense of increased water usage and the consequent decrease in thermal effectiveness [see equation (10)]. Below $Ja = 1$ there is insufficient thermal capacity in the water to condense 100% of the incoming steam. For $Ja < 1$, F rapidly tends to zero. As discussed above, fraction condensed is very sensitive to $X_{i,i}$, ΔT_c and S. As a result of logistics relating to the system layout and coupling effects between the components of the vacuum train, it was not possible to establish identical conditions over multiple runs to maintain these critical parameters constant while varying only the Jakob number. Nevertheless, nine cases near the previously stated inlet conditions are shown in the same figure for comparative purposes. Each of these nine cases is represented by a data point paired with its individual model prediction and represents a slightly different set of inlet conditions. At each individual model prediction point, a curve similar to the one shown would be calculated by the model. As the inlet conditions change slightly for each of the nine cases, this curve will shift down as ΔT_c decreases and up as $X_{i,i}$ decreases. Therefore, the scatter of these nine cases about the one curve shown are irrelevant and only the difference between each datum and its corresponding model prediction should be considered.

Heat-exchange effectivenesses inferred from the model predictions of $T_{g,o}$ were found to be generally above 0.9. In all tests, the gas pressure drop through the packing remained very low (see Table 1), because of the relatively low gas loadings (low gas velocities). Although the error in ΔP is large, the model predicts values within a standard deviation of ± 24 Pa from all measurements. Temperature distributions within the exchanger follow the same trends discussed in [5], except that the inlet superheat is considerably larger in these tests. Outlet superheat can be inferred from $\varepsilon_h \approx 0.9$.

The exhaust performance indicates how effective the IC is in removing the maximum possible quantity of steam from the gas. It can be expressed in terms of the vent ratio [4], which depends on total gas pressure drop and approach between steam dew point and cold seawater temperature at the gas outlet. Because the gas pressure drop is small at the operating pressures tested in the ICs, the exhaust performance is presented in Fig. 5 in terms of the approach, $(T^*_{dew,o} - T_{w,i})$, against the Jakob number. Only data from IC3 and IC4 were selected, because of the smaller fluctuations in dew points. $X_{i,i}$ ranges between 0.52 and 0.88, so there is still significant scatter, but the trend is noticeable. The negative numbers are not physically possible and result from measurement errors. The solid line in Fig. 5 represents the outer envelope that delimits the highest values predicted by the model, for all data points shown.

Simple condensers operating with seawater attain approaches near zero for $Ja_0 \approx 1.2$ [4]. The data in Figs. 4 and 5 may infer that, when high superheat and $X_{i,i}$ are present, the exchangers approach the ideal conditions at higher Ja than for simple condensers; however, the new data are insufficient to validate this conjecture.

CONCLUSIONS

The tests significantly broadened the range of pressures, superheat and inlet noncondensible gas concentrations at which direct-contact heat and mass exchangers have been tested. These units continued to

demonstrate good thermal and exhaust performance, attaining fraction condensed within 0.05 of the theoretical limit, and also indicating heat-exchanger effectiveness around 0.9. Condensing effectiveness is a function of Jakob number selected. For typical power-plant conditions, a fraction condensed of about 0.95 is attainable with a Jakob number around 1.2, giving a condensing effectiveness of about 0.9.

The computer models predicted the experimental fraction condensed to within a standard deviation of ± 0.046 across the range tested; this is excellent agreement for engineering design. Although the conditions typical of geothermal and conventional power plants could not all be attained simultaneously during these tests (e.g. high inlet pressures with high steam loadings and very low noncondensible fractions), it is expected that the exchangers will perform as predicted by the model under the less severe conditions (very low NC) to be encountered in those applications. Thus, the models can now be used with confidence to design direct-contact condensers and heat exchangers at the operating pressures encountered in these applications.

The performance of direct-contact heat and mass exchangers is very sensitive to parameters such as noncondensible gas fraction, temperature driving potential, steam loading, and Jakob number, and the computer models are necessary to carry out an engineering design. However, for moderate steam loadings, the performance can be estimated using the ideal limits presented in this paper, which simplifies the initial conceptual design effort.

Regarding the practical operation of the ICs at the test facility, their performance is quite good. Smaller-diameter intercoolers could have been used without significant performance penalties; higher gas loadings were proposed in the conceptual design. The coldest seawater available in the plant should be used in the intercoolers, to remove the maximum possible amount of steam before each stage of compression. For the same reason, Jakob numbers near 2 are recommended, considering that only small quantities of seawater are required.

Acknowledgements—Sincere thanks are owed to the operators of the test facility, Joe Clarkson, Peter Shackleford and Joe McClesky, who provided invaluable help and interesting discussions during the experiments. The authors also wish to acknowledge the financial support received from the U.S. Department of Energy, Ocean Energy Technology Program, and the support for the sabbatical assignment received from the Spanish Interministry Commission of Science and Technology, and from the Complutense University.

REFERENCES

1. H. R. Jacobs, Direct-contact heat transfer for process technologies, *ASME J. Heat Transfer* **110,** 1259–1270 (1988).
2. J. R. Fair, Direct contact gas–liquid heat exchange for energy recovery, *ASME J. Solar Energy Engng* **112,** 216–222 (1990).
3. D. Bharathan, B. K. Parsons and J. A. Althof, Direct-contact condensers for open-cycle OTEC applications: model validation with fresh-water experiments for structured packings, SERI/TR-252-3108, Solar Energy Research Institute, Golden, CO (October 1988). U.S. Government publications can be ordered from NTIS, 5285 Port Royal Road, Springfield, VA 22161.
4. F. Zangrando, D. Bharathan, H. J. Green, H. F. Link, B. K. Parsons, J. M. Parsons, A. A. Pesaran and C. B. Panchal, Results of scoping tests for open-cycle OTEC components operating with seawater, SERI/TP-253-3561, Solar Energy Research Institute, Golden, CO (September 1990).
5. F. Zangrando and D. Bharathan, Direct-contact condensation of low-density steam on seawater at high inlet noncondensible concentrations, *ASME J. Heat Transfer* **115,** 690–698 (1993).
6. L. A. Vega and D. E. Evans, Operation of a small OC-OTEC experimental facility, *Proceedings of Oceanology International* '94, Vol. 5, Brighton, U.K. (8–11 March 1994).